Engineering motile aqueous phase-separated droplets via liposome stabilisation

Shaobin Zhang
Department of Chemistry, Imperial College London, Molecular Sciences Research Hub, Shepherd's Bush, London, W12 0BZ, UK

Claudia Contini
Department of Chemistry, Imperial College London, Molecular Sciences Research Hub, Shepherd's Bush, London, W12 0BZ, UK

James Hindley
Department of Chemistry, Imperial College London, Molecular Sciences Research Hub, Shepherd's Bush, London, W12 0BZ, UK AND Institute of Chemical Biology, Imperial College London, Molecular Sciences Research Hub, Shepherd's Bush, London, W12 0BZ, UK AND fabriCELL, Imperial College London, Molecular Sciences Research Hub, Shepherd's Bush, London, W12 0BZ, UK https://orcid.org/0000-0002-3392-4387

Guido Bolognesi
Department of Chemical Engineering, Loughborough University, Loughborough, LE11 3TU, UK
https://orcid.org/0000-0002-2380-0794

Yuval Elani
Institute of Chemical Biology, Imperial College London, Molecular Sciences Research Hub, Shepherd's Bush, London, W12 0BZ, UK AND fabriCELL, Imperial College London, Molecular Sciences Research Hub, Shepherd's Bush, London, W12 0BZ, UK AND Department of Chemical Engineering, Imperial College London, South Kensington, London, SW7 2AZ, UK

Oscar Ces (✉ o.ces@imperial.ac.uk)
Department of Chemistry, Imperial College London, Molecular Sciences Research Hub, Shepherd's Bush, London, W12 0BZ, UK AND Institute of Chemical Biology, Imperial College London, Molecular Sciences Research Hub, Shepherd's Bush, London, W12 0BZ, UK AND fabriCELL, Imperial College London, Molecular Sciences Research Hub, Shepherd's Bush, London, W12 0BZ, UK

Article

Keywords: motile aqueous phase-separated droplets, liposome stabilization, artificial cell construction, motility

Posted Date: July 10th, 2020

DOI: https://doi.org/10.21203/rs.3.rs-37639/v1

Version of Record: A version of this preprint was published at Nature Communications on March 15th, 2021. See the published version at https://doi.org/10.1038/s41467-021-21832-x.

Engineering motile aqueous phase-separated droplets via liposome stabilisation

Shaobin Zhang[1], Claudia Contini[1], James W. Hindley[1,2,3], Guido Bolognesi[4], Yuval Elani[2,3,5], Oscar Ces[1,2,3]*

1. Department of Chemistry, Imperial College London, Molecular Sciences Research Hub, Shepherd's Bush, London, W12 0BZ, UK
2. Institute of Chemical Biology, Imperial College London, Molecular Sciences Research Hub, Shepherd's Bush, London, W12 0BZ, UK
3. fabriCELL, Imperial College London, Molecular Sciences Research Hub, Shepherd's Bush, London, W12 0BZ, UK
4. Department of Chemical Engineering, Loughborough University, Loughborough, LE11 3TU, UK
5. Department of Chemical Engineering, Imperial College London, South Kensington, London, SW7 2AZ, UK.

* Correspondence: o.ces@imperial.ac.uk

Abstract

There are increasing efforts to engineer functional compartments that mimic aspects of cellular behaviour in a drive to construct an artificial cell from the bottom-up. One behaviour that is receiving particular attention is motility, due to its biotechnological potential and the fact that movement of discrete cells is a ubiquitous feature of living systems. Many existing platforms make use of the Marangoni effect to achieve motion in water/oil (w/o) droplet systems. However, most of these systems are unsuitable for biological applications due to issues with biocompatibility caused by the presence of oil phases. Here we report a biocompatible all aqueous (w/w) PEG/dextran Pickering-like emulsion system consisting of liposome-stabilized cell-sized droplets, where the stability can be easily tuned by adjusting liposome composition and concentration. We demonstrate that the compartments are capable of negative chemotaxis: if water is introduced into the emulsion system, these droplets can respond through directional

motion away from PEG in the continuous phase and down to the polymer gradient with a velocity change proportional to the rearrangement of liposome stabilisers in the PEG/dextran interface. The biocompatibility, motility and partitioning abilities of this novel droplet system offers new directions to pursue research in motion-related biological processes.

1 Introduction

The development of motile cell-mimetic compartmentalised systems is receiving increasing interest due to their potential in applications including targeted drug delivery[1, 2, 3] and environmental restoration[4, 5]. The fact that controlled motility and chemotaxis is a behaviour that is considered to be one of the hallmarks of life has also made it a focus in the endeavour to construct artificial cells that mimic biological cells in form and function[6, 7]. To propel an object, various strategies have been exploited such as bubble-propulsion[8, 9, 10], diffusiophoresis[11, 12, 13, 14, 15], magnetic force[16, 17], and the Marangoni effect[18, 19, 20]. Among these methods, the Marangoni effect is a commonly used way to induce motion since it can be easily achieved[3]. The asymmetric distribution of interfacial tension (IFT) around a droplet spontaneously generates a Marangoni flow on the droplet surface, driving its motion. A typical example of the Marangoni effect can be achieved by adopting a water/oil system, in which a water or oil drop can move in an oil or aqueous phase respectively by responding to changes in the droplet IFT [3, 21, 22, 23]. For example, Xiao et al.[3] reported that by adding photo-active surfactant precursors to an oil droplet, motion can be produced in an aqueous phase if one side of the oil droplet is irradiated by a light source to initiate a photo-responsive chemical and then generate an asymmetrical distribution of IFT. Li et al.[23] reported that water/ethanol droplets can achieve motion in an oil phase containing squalene/monoolein. In their system, water/ethanol droplets transform into Janus droplets in the oil phase by separating into water-rich and ethanol-rich part components. Monoolein holds affinity to the ethanol-rich part, which leads to IFT difference between the water-rich part and the ethanol-rich part, generating a

Marangoni flow and subsequent motion. However, with these water/oil systems, biocompatibility is an inevitable problem for those due to the existence of oil phases, which limits their applications in biotechnological settings. In contrast, water/water systems are ideal candidates for bio-related research because of their intrinsic biocompatibility. However, there are few examples about using water/water systems to produce motile droplets, and the stability and controllability of those motile water/water systems are inadequate[24, 25]. Thus, there is a need to develop novel stable and controllable motile systems based on water/water systems.

The aqueous two-phase system (ATPS) is a common water/water system that forms when two polymers (such as polyethylene glycol (PEG) and dextran (DEX)) are co-dissolved in water[26, 27]. In the aqueous solution, the polymer molecules segregate at high concentrations due to the poor entropic gain from polymer mixing. This causes separation into two phases (affected by pH, temperature, and molecular weight of polymers)[28, 29, 30]. Both aqueous phases in ATPS have similar properties with the cell cytoplasm such as high viscosity as they are all composed of macromolecule assemblies produced through phase separation[31]. Apart from that, these two phases usually hold different physical and chemical properties, the difference of which allows their exploitation for separation and purification of biomolecules[27]. For example, natural proteins, DNA, and urease prefer to diffuse into the DEX-rich phase while denatured proteins normally accumulate in the PEG-rich phase[32, 33]. It is also reported that compartmentalisation can be accomplished in a liposome-stabilized ATPS-based emulsion system[34], which provides a new method for designing artificial cells and organelles. Therefore, ATPS is an attractive system for many bio-related areas such as molecule separation[35, 36] and control of biomolecular reactions[37].

Here we report a novel biocompatible motile emulsion droplets system by combining the Marangoni effect with ATPS. The emulsion system is composed of PEG/DEX ATPS[33, 36, 37, 38, 39]. To stabilize these emulsion droplets, PEGylated liposomes are used as a droplet stabilizer.

Once emulsion droplets are obtained, a liposome coating is formed on their surface which stabilises the system. By introducing a polymer gradient into this emulsion system, the aqueous droplets achieve motion as a result of the Marangoni effect. This motion is modulated by the liposomal stabiliser: in response to the polymer gradient, the liposome coating will gradually become asymmetric generating an IFT imbalance across the droplet that weakens the Marangoni effect. Such an effect acts as a dampener, increasing the controllability of droplet motion. Since both its lumen and outer environment are fully aqueous, and possess cytoplasm-like properties, this novel motile droplet not only can act as a carrier for cargo delivery within biological environments but also serve as a platform to research motility-related cellular phenomena.

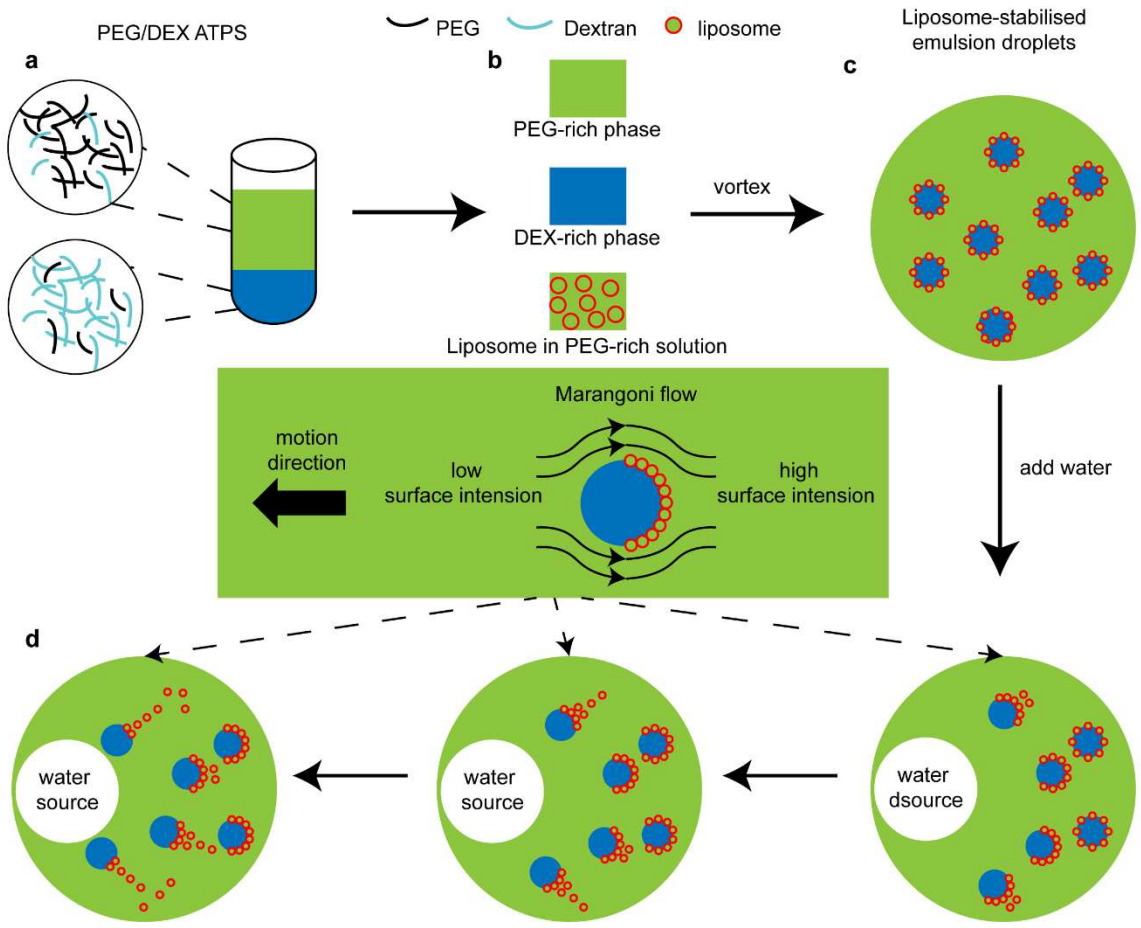

Fig.1 Illustration for the main content. (a) PEG/DEX solution separates into PEG-rich and DEX-rich phase. **(b)** Preparation of liposome in PEG-rich solution. **(c)** Preparation of emulsion droplets by mixing PEG-rich phase, DEX-rich phase, and liposomes via vortex. **(d)** Droplets achieve directional motion towards the water source in respond to a polymer gradient caused by the addition of water.

Results

Droplet structure and stability

The ATPS in our research consists of PEG (10 wt/wt %), dextran (16 wt/wt %), and water (74 wt/wt %). After phase separation, two clear phases can be obtained: the upper is a PEG-rich phase while the lower is a DEX-rich phase[37] (Supplementary Table 1). Water-in-water emulsions can be obtained by simply mixing PEG-rich phases and DEX-rich phases via vortex. In our case, droplets consisting of a DEX-rich (dispersed phase) are immersed in a PEG-rich phase (continuous phase). To verify the emulsion bulk stability, a UV-vis spectrometer was used to monitor the emulsion turbidity by measuring the absorbance of formed emulsions. We take the ratio of measured absorbance at each time point to the absorbance at 0 h as normalized absorbance to better analyse changes in particle size. Fig.2(a) shows that the emulsion absorbance decreases quickly with time when an emulsion was made by simply mixing two aqueous phases, indicating the instability of the generated emulsion. Emulsion droplets are driven to merge to decrease the total surface energy. As a result, a tubid emulsion will gradually reseparate into two clear aqueous phases, causing a decrease in absorbance. Such experiments confirm the necessity of an emulsion stabilizer to generate stable droplets from PEG/DEX solutions.

We chose liposomes for PEG/DEX droplet stabilization as they have been shown to be a good stabilizer for ATPS[34]. In addition, liposomes are capable of encapsulating substances[40, 41, 42] in their lumen, and controllable release can be achieved through the incorporation of phtoto-responsive content such as diacetylene functional groups[41] in liposome composition or membrane proteins such as α-hemolysin[40, 42] in lipid bilayers, which can be exploited to expand the application for chemotaxis. The liposomes used in our research are primarily composed of DOPG phospholipids because the electrostatic repulsion between the DOPG liposomes is beneficial to producing stable droplets. We then investigated the effect of liposome

composition on emulsion stability by varying the molar concentration of PEGylated lipids in liposomes. As shown in Fig.2(a), the absorbance of emulsions stabilized by unPEGylated DOPG liposomes shows the same trend with time as that of the emulsion made without liposomes,indicating that unPEGylated liposomes are unsuitable for emulsion droplet stabilisation. After being added into ATPS, unPEGylated liposomes do not prevent droplet coalescence and therefore cannot stabilize the emulsion. We attributed this phenomenon to the partition preference of unPEGylated liposomes to the DEX-rich phase (droplet lumen)[34]. To adjust liposome partition preference and to provide additional steric stabilization of droplets, we added different amounts of DOPE-PEG2k lipids into the liposome formulation. Fig.2(a) shows that with PEGylated liposomes, the emulsion absorbance shows limited change in 8 hours, indicating that the emulsions are stable during the observational period. To quantitively analyse emulsion stability, we compared the normalized absorbance 8 hours after preparation. It shows that emulsion stability increases with the concentration of PEGylated lipids and reaches a maximum at 1.5 mol%. After this point, a further increase in the PEGylated lipid concentration will lead to a gradual decrease in emulsion stability. With the increase of PEGylated lipid concentration, liposome partitioning preference gradually changes from the DEX-rich phase to PEG-rich phase[34]. When the concentration of PEGylated lipid is below 1.5 mol%, increased partition preference to the PEG-rich phase will cause liposomes to gradually move from the DEX-rich phase (droplet lumen) to the PEG-rich phase of the droplet interface, resulting in increased emulsion stability. Once the concentration is above 1.5 mol%, liposomes partition further into the PEG-rich phase, leading to a decreased emulsion stability. Hereafter, it can be assumed that 1.5 mol% PEGylated liposomes are used to produce all further emulsions unless explicitly stated.

It is reported that PEGylated liposomes will remain at the droplet interface and form a barrier[34] in liposome-stabilized emulsions (Fig.2(b)). To verify the droplet structure, we added DOPE-

Rh lipids in liposomes to monitor their position. Calcein was encapsulated in rhodamine-dye PEGylated liposomes to further help locate and monitor the intactness of liposomes. These liposomes were purified via size exclusion chromatography before use to exclude any unencapsulated calcein (Supplementary Fig.2). The resulting purified liposome solution was then used to form emulsion droplets by mixing it with ATPS, and the emulsion observed using a microscope under calcein and rhodamine channels. As shown in Fig.2(c), the edge of the droplets is bright while the lumen is relatively dark, which means that liposomes remain at the droplet surface when stabilizing the emulsion. In addition, the images obtained from the calcein channel overlap with the image obtained in the rhodamine channel, proving that liposomes keep intact when forming a barrier. Hereafter, all liposomes contain DOPE-Rh to aid observation via fluorescence microscopy, and droplet pictures are captured in the rhodamine channel unless explicitly stated.

To investigate droplet stability, we prepared different emulsions by varying the liposome concentration from 0.05 mg/mL to 0.20 mg/mL, and then measured the droplet size every 12 minutes within a period of 120 minutes (Supplementary Fig.3). As shown in Fig.2(d), the initial droplet size is nearly the same despite the liposome concentration being changed. This is because the initial droplet size is only dependent on the mixing strength during the emulsion formation. Droplet size increases with time, and a higher liposome concentration corresponds to a faster increase in droplet size causing a significant difference in droplet size after 2 hours. At this time, the droplet diameter for 0.05 mg/mL is nearly double that for 0.10 mg/mL and nearly four times bigger than that for 0.15 and 0.20 mg/mL. Moreover, for concentrations above 0.05 mg/mL, a plateau region can be observed, and the time needed for reaching the plateau stage decreases with liposome concentration (72 minutes for 0.15 or 0.20 mg/mL versus 96 minutes for 0.10 mg/mL). The assumption was made that a minimum coverage is necessary to create stable droplets. This coverage can be defined with the liposome surface concentration

that is the ratio of the number of liposomes at droplet surface to droplet surface area (see Supplementary Information for detailed calculation). At the beginning of the observation, the surface concentration is not high enough to prevent droplet coalescence although a liposome barrier can be formed around DEX-rich droplets at the interface. As a result, frequent droplet coalescence occurs after emulsion formation with a consequent rapid increase of droplet size. The surface concentration increases as droplets merge, and droplets become stable enough to resist coalescence once the surface concentration is above the threshold. As a result, the droplet size remains unchanged (plateau stage in Fig.2(d)). When the liposome concentration increases from 0.05 mg/mL to 0.20 mg/mL, the surface concentration at 0 min increases as well, thus fewer coalescence events are needed for reaching the threshold surface concentration and less time is needed to reach the plateau. Fig.2(e) shows the droplet size distribution when droplets become stable (at 120 min for 0.10 mg/mL).

We then further investigated the effect of liposome composition on droplet stability. Liposomes containing DOPC (zwitterionic) or DOPG (anionic) lipids were used to generate emulsion droplets with the liposome concentration fixed at 0.10 mg/mL. Fig.2(f) demonstrates that the size of DOPG-droplets reaches a stable stage within 96 minutes after formation while that of DOPC-droplets keeps changing even 2 hours after formation, showing that DOPG-droplets are more stable at the same liposome concentration. We attribute this stability variance to the difference in the charge between DOPG lipids and DOPC lipids. When liposomes are composed of DOPG lipids, electrostatic repulsion will exist between the liposomes, and this repulsion will cause an increased distance between liposomes. Therefore, compared with DOPC-droplets, less liposomes are needed to cover the surface of DOPG-droplets, resulting in less coalescence events (and the time) necessary to produce stable droplets. To further confirm the electrostatic stabilisation of droplets with charged liposomes, the emulsion stability was investigated in the presence of salt. Sodium chloride (NaCl) was added into the PEG-rich phase

before mixing, with the preparation of emulsions as previously stated. When NaCl was added into the emulsion, DOPG-droplet diameter at 120 min significantly increases (117.6% increase,Fig.2(f)) whilst the DOPC-droplets' diameter undergoes a much smaller increase (increased 14.5%, Fig.2(f)). This indicates that NaCl has a much bigger effect on DOPG-droplet stability. As mentioned above, electrostatic repulsion between DOPG-liposomes is beneficial for stabilising droplets. However, salt addition shields the electrostatic repulsion between DOPG-liposomes due to "charge screening" effect within the emulsion. Thus, the stabilisation pass from electrostatic to steric in nature with a significant reduction of the distance between DOPG-liposomes. This greatly reduces the surface area that can be covered at a fixed liposome concentration and leads to a large reduction in DOPG-droplet stability. As a consequence, increased merging occurs within the same time duration, causing a large change in droplet diameter at 120 min. In comparison, the electrostatic interactions between zwitterionic DOPC liposomes are reduced. The small decrease in droplet stability can be accredited to the "water removal" effect of salt addition rather than a change in the nature of droplet stabilisation. The addition of NaCl in PEG-rich removes water between liposomes[43], and this reduces the distance between liposomes and subsequently, the droplet stability.

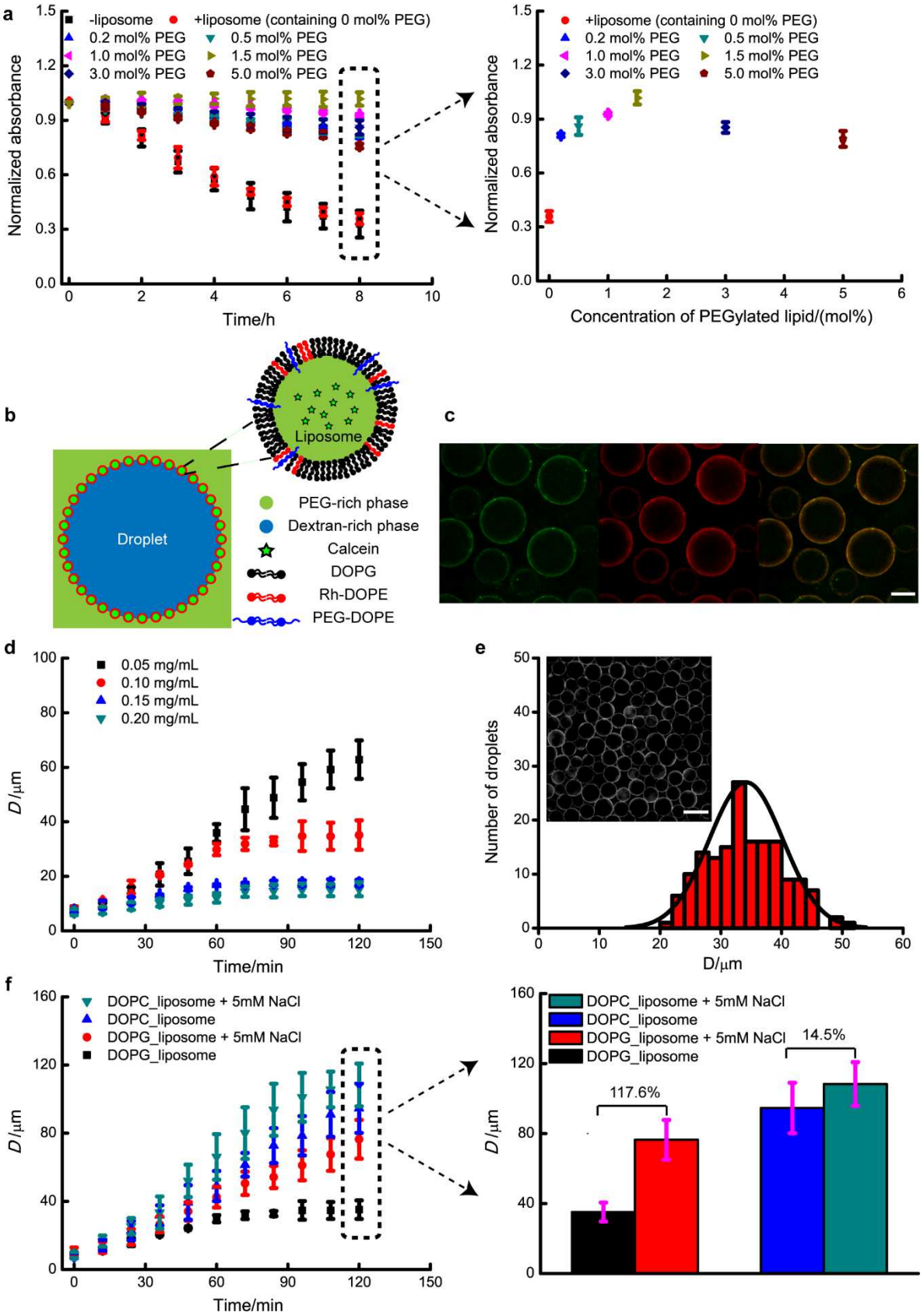

Fig.2 Characterisation of droplet morphology and stability. (a) Emulsion absorbance change during 8 h. If emulsions stay stable, it should remain turbid during observation, i.e. the absorbance remain unchanged. Or a decrease in absorbance can be observed for unstable emulsions. Final absorbance at 8 h was extracted for quantitative analysis. **(b)** Illustration for liposome-stabilise droplet. **(c)** Droplets stabilized by Calcein-containing (5mM) liposomes. From left to right, Calcein channel, Rhodamine

channel, and merger channel. Colours were added via Image J. Liposome solution is diluted after size exclusion, which leads to the large droplet size. Scale bar is 50 μm. **(d)** Effect of liposome concentration on droplet stability. **(e)** Droplet size distribution for stable droplets (stabilised with DOPG-liposomes). The inset picture corresponds to droplets at 120 min for 0.10 mg/mL in (d). Scale bar is 50 μm. **(f)** Effect of liposome type and salt addition on droplet stability. Droplet diameter at 120 min was extracted to draw a histogram in order to show the difference of salt addition on different liposome-stabilised droplets. Error bars represent 1 s.d. (n = 3) for each data set.

Directional droplet motion

DOPG-droplets were prepared with a 0.1 mg/mL liposome concentration and then transferred into an observation chamber. The emulsion was then left for 1 hour to equilibrate. We then added 50 μL water to one side of the chamber (see Fig.3(a)). This led to the creation of a polymer gradient (∇c_P). In response to this, we observed that the PEG/DEX emulsion droplets transformed from homogenously fluorescent droplets into asymmetric Janus droplets, where only the region of droplets further away from the water source is fluorescent (Fig.3(a), Supplementary Video 1-3). We note that Janus droplets aligned with the relative location of the water source, and along the polymer gradient: the droplet hemisphere closer to the water source (front side) is dark while the other part (rear side) is bright, as shown in Fig.3(a). Fig.3(b) shows Janus droplets remain intact spherical structure under bright field, which means the transformation of PEG/DEX droplets is caused by changes in the liposome coating on the surface of the PEG/DEX emulsion droplets. The total fluorescence intensity of liposome coating during the transformation in Janus structures was roughly constant (Supplementary Fig(4)). This indicates that the formation of Janus droplets is due to the rearrangement of liposomes on the droplet surface rather than the loss of liposomes in PEG-rich phase. As shown in Fig.3(c), this transformation can be monitored by observing how the height of non-fluorescent portion of the droplet (h) changes during the structural transformation. We then define ε as the ratio of h to D (droplet diameter) to quantitatively characterise the Janus structure for each droplet.

As a control, we found that adding a PEG-rich phase instead of a water solution simply causes limited droplet merging within the local vicinity, while adding more of the DEX-rich phase eliminates a great number of emulsion droplets within the chamber (Supplementary Fig(5), Video 4 and 5). No formation of asymmetric Janus droplets or motility was observed in either case.

We found that motility started when the droplets reached a Janus structure corresponding to approximately $\varepsilon \sim 0.3$. At this point, droplets started moving toward the water source with a fluorescent tail following at the rear side of droplets indicating a loss of droplet-associated liposomes (Fig.3(c)). Fig.3(d) shows the trajectories of moving droplets are directional, and droplet trajectories are nearly parallel to each other. Moreover, the direction of movement aligned with the axis of symmetry of the Janus structure. As shown in Fig.3(e), the droplet velocity increased with time during motion. The mean square displacement (MSD)-time curves for moving droplets are not linear (Fig.3(f)), indicating the droplet motion is not random diffusion. In addition, droplet diameter did not change significantly during motion, as shown in Fig.3(g).

The Marangoni effect can be used to explain the topology changes and the directional motion observed. It has previously been reported that in the absence of liposomes the formation of a polymer gradient creates an IFT gradient ($\nabla\gamma_P$) since the IFT between PEG-rich phase and DEX-rich phase changes with polymer content in ATPS[44]. As a result, the two poles of the droplet close to and away from the water gradient experience different IFTs. This imbalance induces a Marangoni flow on the droplet surface (from front side to rear side). In our experiments, where liposomes reside at the interface, this flow leads to the change in the liposome coatings on the droplets surface, and a change from a homogeneously coated droplet to one with an asymmetrical distribution. The asymmetrical liposome coating will cause an IFT gradient ($\nabla\gamma_L$) in the opposite direction that balances the water-induced IFT gradient, leading

to the immobilisation of the droplet interface. As a result, droplets cannot initially achieve motion. Only when the ε of Janus structure reaches approximate 0.3, does the $\nabla\gamma_L$ cannot balance $\nabla\gamma_P$, so droplets begin their directional motion towards the water source. During droplet motion, liposomes are gradually lost from droplets due to surface flow, generating a liposome tail to the rear side of the droplets (Supplementary Videos 1-3).

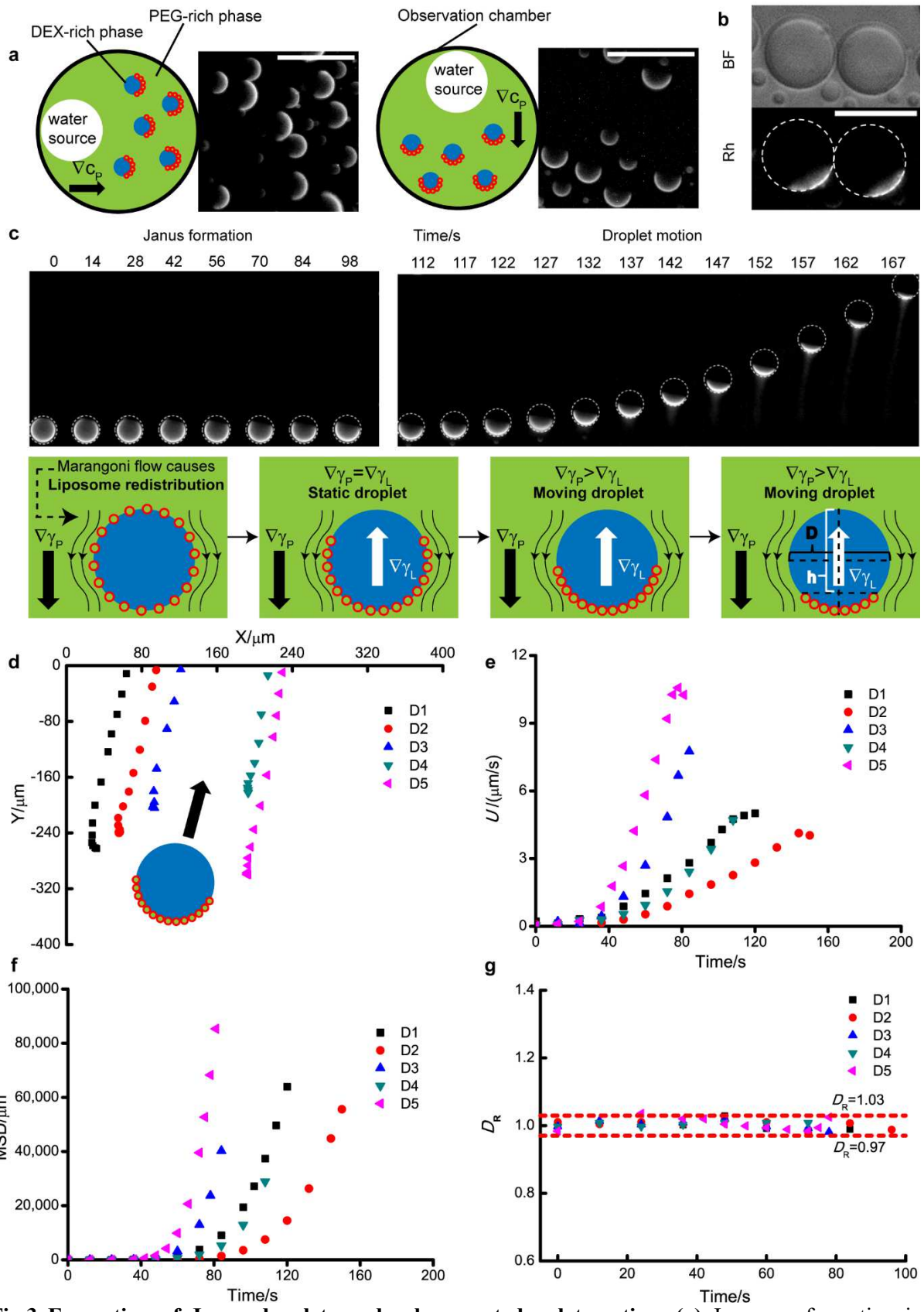

Fig.3 Formation of Janus droplets and subsequent droplet motion. (a) Janus conformation is relevant with the position of water addition. Pictures were extracted from video 1 and 2 and cropped for better presentation. ∇_{C_P} is the polymer gradient. **(b)** Droplet structure under bright field (BF) or Rhodamine fluorescence channel (Rh). **(c)** Janus formation and droplet motion. In respond to water gradient, the droplet gradually transformed into Janus droplet. When the ratio of h to D reached

approximate 0.3, the droplet starts a directional motion towards the water source, with a characteristic tail of liposomes due to liposome desorption from the droplet surface during the motion. ∇_{γ_P} and ∇_{γ_L} are the IFT gradients caused by polymer gradient and liposomes respectively. Frames were extracted from video 1 and cropped for better presentation. **(d)** Trajectories of moving droplets. D1-D5 are representative droplets stochastically chosen from video 1. Arrow corresponds to the direction of movement. **(e)** Corresponding velocity , **(f)** MSD and **(g)** diameter change (the ratio of droplet diameter at different time points to its average diameter during motion was taken as normalized diameter, i.e. D_R) for droplets in (d). The time points when droplets start moving were chosen as time zero. Scale bar is 50 μm for (a)-(c).

Analysis of droplet motion

For a qualitative analysis of droplet motion, we can model the droplet surface as a sharp (not diffuse) interface with an IFT γ that depends on the total polymer concentration c_P and the surface concentration σ(see Supplementary Information for more detail). Cartesian ($\boldsymbol{e_x}, \boldsymbol{e_y}, \boldsymbol{e_z}$) and spherical ($\boldsymbol{e_r}, \boldsymbol{e_\theta}, \boldsymbol{e_\phi}$) coordinate systems are defined with the origin at the droplet centre and z axis parallel to the total polymer concentration gradient, so that $\nabla c_P = \frac{\mathrm{d}c_P}{\mathrm{d}z}\,\boldsymbol{e_z}$. Since the IFT γ increases with c_P[44], in the absence of liposomes droplets would migrate towards lower polymer concentration regions due to the Marangoni effect at a speed of

$$\boldsymbol{U} = \frac{-D}{2(2\mu_o + 3\mu_i)}\,\frac{\mathrm{d}c_P}{\mathrm{d}z}\,\Gamma\boldsymbol{e_z} \tag{1}$$

where μ_o (μ_i) is the viscosity of the outer (inner) phase and both $\frac{\mathrm{d}c_P}{\mathrm{d}z}$ and $\Gamma \simeq \left(\frac{\partial\,\gamma}{\partial\,c_P}\right)$ are assumed to be constant during droplet motion on the time scale of experimental observation. Eq. (1) can be derived by solving the Stokes equations for the dispersed and continuous phase and imposing the balance of tangential stresses at the droplet surface $\tau_{r\vartheta}^{(i)} - \tau_{r\vartheta}^{(o)} = \nabla\gamma \cdot \boldsymbol{e_\theta}$, where $\tau_{r\vartheta}^{(i)}$ and $\tau_{r\vartheta}^{(o)}$ are the tangential stress at the droplet surface exerted by the inner and outer phase, respectively (see Supplementary Information for more detail). In presence of liposomes, droplet motion still occurs in the same direction but liposomes accumulate at the rear end of the droplet due to fluid motion at the droplet interface, as shown in Fig.3(c). To a first

approximation, this configuration can be modelled as shown in the schematic in Fig.4(a). In the region $\theta < \bar{\theta}$, there are no absorbed liposomes and the corresponding IFT can be denoted as $\gamma_0(\theta) = \gamma(c_p(\theta), \sigma = 0)$, whereas in the region $\theta \geq \bar{\theta}$, there are absorbed liposomes at a surface concentration σ and the corresponding IFT in this region is denoted as $\gamma_L(\theta, \sigma) = \gamma(c_p(\theta), \sigma)$. Due to the spontaneous absorption of liposomes at the droplet interface, the IFT decreases with the liposome surface concentration and hence $\gamma_L(\bar{\theta}) < \gamma_0(\bar{\theta})$. As a result, the liposome distribution induces Marangoni-stresses at the droplet interface, proportional to $\Delta\gamma(\sigma) = \gamma_0(\bar{\theta}) - \gamma_L(\bar{\theta})$, that counteracts the effect of the total polymer concentration gradient ∇c_P. As the liposomes are swept towards the rear end, the opposing Marangoni force increases (as both σ and $\Delta\gamma(\sigma)$ increase) and the motion of the droplet is retarded. This behaviour is analogous to the well-known surface immobilisation effect for a rising bubble in a surfactant solution[45, 46, 47, 48]. However, once the maximum liposome surface concentration σ is achieved, the liposomes are expelled from the droplet interface, due to repulsive electrostatic interactions, and the intensity of the opposing Marangoni force approaches its peak. Finally, the droplet sets into motion while liposomes are ejected from the rear end. As liposomes are removed from the droplet interface, the opposing Marangoni force decreases and the droplet velocity increases towards the peak value U_{max}, given by Eq. (1) that holds for a droplet with a "clean" surface, namely without liposomes at the interface (i.e. $\theta = \pi$ and $\varepsilon = 1$).

The proposed physical description of the droplet motion is consistent with the experimental observations. As shown if Fig.4(b), the droplets do not set into motion as long as the liposomes remain attached to the droplet interface and are accumulated towards the droplet rear end ($\varepsilon > 0$) due to the opposing effects of the interfacial tension gradient $\frac{\partial \gamma}{\partial c_P}$ and the interfacial tension contrast, $\Delta\gamma(\sigma)$. As the liposomes are ejected from the droplet interface, the droplets move at an increasing speed until this reaches a peak value U_{max}. Fig.4(c) shows that U_{max} increase linearly with the droplet diameter, as predicted by Eq.(1). Furthermore, Eq.(1) predicts, under

the examined experimental conditions, a maximum speed of $U_{max} \simeq 10$ μm /s for a 20μm droplet, which agrees well with the experimental observations – see Fig.4(c). Since the opposing Marangoni force is only determined by ε (both σ and $\Delta\gamma(\sigma)$ are solely determined by ε), then the droplet velocity only changes with ε. We defined the normalized velocity (U_R) as the ratio of droplet velocity at each ε to its maximum velocity, and Fig.4(d) shows that the U_R-ε curve is roughly overlapped for different droplets, fitting well with the theory.

By using scaling arguments, it can be shown that the linear relationship between droplet speed and diameter holds for any droplet velocity, and not just for the peak velocity. Indeed, the force F_M induced by Marangoni stresses, driven by ∇c_P and σ, is proportional to the droplet surface area, $F_M \propto D^2$, whereas the viscous drag F_D is proportional to $U\,D$. From the force balance $F_M = F_D$, it follows $U \propto D$. Additionally, for droplets within the same region of the sample, one can expect that they are exposed to the same polymer concentration gradients ∇c_P. If, then, droplets have similar values of ε, the ratio U/D should also be similar, and thus the bigger droplets should exhibit a larger velocity. This behaviour is confirmed by Fig.4(e) which shows the chasing process of a big droplet (droplet A) to a small droplet (droplet B). As shown in the figure, the distance between these two droplets gradually decreases with time during the first 6 s. When droplet A collides into droplet B, they merge into a new larger droplet (droplet C) with a symmetrical liposome coating (9-12 s Fig.4(e)). This symmetrical liposome coating gradually turns into an asymmetric one, driving the transformation of droplet C into a Janus droplet (12-15 s in Fig.4(e)). Droplet C is stationary during the transformation process, and it starts moving and accelerating only after droplet C becomes a Janus droplet (18-24 s in Fig.4(e)). This indicates that recreation of a symmetrical liposome coating on the droplet surface disrupts the asymmetrical IFT distribution around droplet C, impeding droplet motion. As a result, the Marangoni effect is negated until an asymmetric distribution of liposome coating is restored.

To show the dampening effect of the liposome coating on droplet motion, we also undertook motion experiments without liposomes, preparing PEG/DEX emulsion droplets as previous (but without liposome stabilisers). 5 droplets were selected to compare with the 5 droplets in trial 1. As shown in Fig.5, without a liposome coating the droplet velocity shows a sharp increase, indicating a large acceleration. In comparison, for droplets with a liposome coating, the velocity grows gradually, and the onset of this motion is delayed due to the process of Janus formation. These combined effects lead to dramatic differences in the time needed for each droplet species to reach maximum velocity (t_{max}): when droplets move with liposome coating, t_{max} is 94.8 ± 14.2 s (n =5), which is nearly 7 times higher than that for droplets without a liposome coating (13.6 ± 4.1 s, n=5). Such results show the dampening effect of liposome coating of emulsion droplets, which can simultaneously stabilise the droplets as well as help insulate droplet species to the effects of chemical gradients in their local environment.

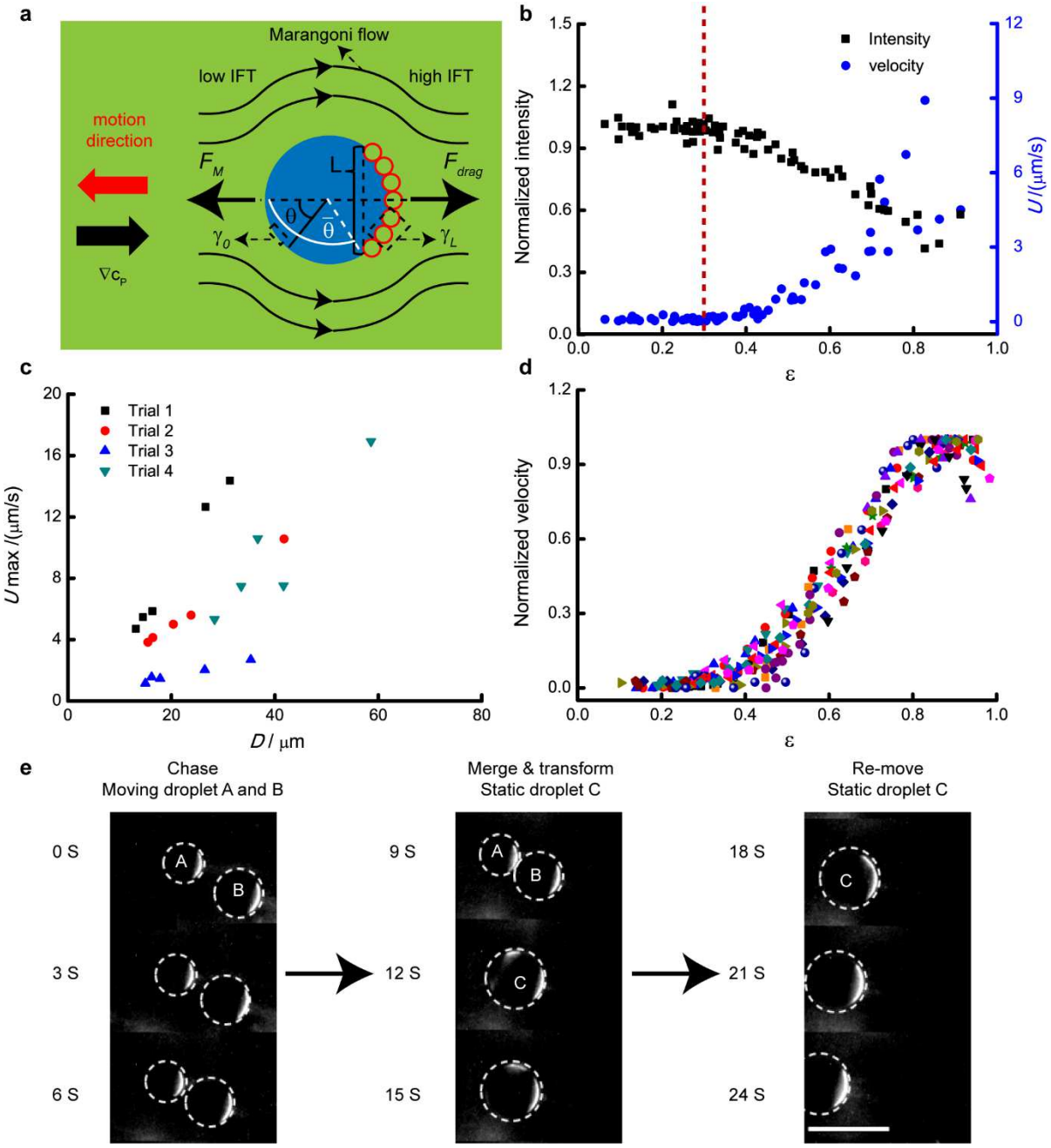

Fig.4 Mechanism behind motion. (a) Illustration for the Marangoni effect. **(b)** The total intensity of liposome coating and corresponding droplet velocity for different droplets. **(c)** The relationship between maximum velocity and droplet diameter. The correlation coefficient for trail 1-4 is 0.99, 0.99,0.96, 0.85. **(d)** The relationship between normalized velocity and the value of ε (h/D). 20 droplets from 4 trials were chosen for analysis. **(e)** Chasing and merge process for two droplets with different diameter. Pictures were extracted from video 6 and cropped for better presentation. Scale bar is 50 μm.

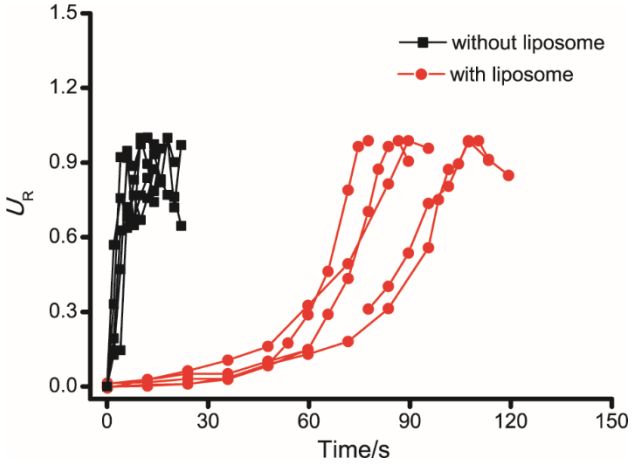

Fig.5 Effect of liposome coating on droplet motion. Emulsion droplets were prepared with/without liposomes, and water was added to induce droplet motion. 5 droplets with or without liposome were chosen from different trials for analysis. The ratio of droplet velocity at different time points to its maximum velocity was taken as relative velocity (U_R).

Discussion

In summary, we have prepared water-in-water emulsion droplets by mixing liposomes with PEG/DEX ATPS. To generate stable emulsions, PEGylated liposomes are needed to act as droplet stabilizers to prevent coalescence, and the optimal content for PEG lipids in liposomes was found to be 1.5 mol%. In our PEG/DEX emulsion system, emulsion droplets are composed of DEX-rich phase, and intact liposomes stay at the droplet interface to form a liposome coating. With an increase in liposome concentration, there are more liposomes on droplet interface, making droplets become more stable. In addition, electrostatic repulsion between liposomes increases the surface area that can be covered at a given liposome concentration, which is beneficial to droplet stability. These droplets achieve structural transformation and then directional motion in response to a concentration gradient formed by the addition of water. The trajectory of this motion is a strongly directional, occurring down the polymer gradient (and perpendicular to the cross-section of the liposome coating). During movement, droplet velocity gradually increases to a maximum, which fits well with theoretical analysis.

Our platform combines the stabilising effect of the interfacial liposome coating, with Marangoni-driven motility and chemotaxis. Importantly, we show the liposomes themselves

can act as engineering control elements, and act as dampening modulators to control both the onset of motion as well as droplet acceleration, making this motile system more controllable. In addition, the presence of lipid membranes associated with the droplet paves the way for the incorporation of membrane-associated biomolecular machinery in future. Finally, given both droplet lumen and outer aqueous environment are cytoplasm-like high viscous environment, our system holds great potential in researching motion-related cellular process. For example, signalling biomolecules can be encapsulated within droplet lumen and delivered to natural cells that locate at outer aqueous environment to trigger specific cellular activities, mimicking intercellular communication.

Methods

Materials

PEG 8 kDa was purchased from Fisher Scientific (P1563) and Dextran 10 kDa from Sigma Aldrich (D9260). 1,2-dioleoyl-sn-glycero-3-phospho-(1'-rac-glycerol) (sodium salt) (DOPG, 840475), 1,2-dioleoyl-sn-glycero-3-phosphoethanolamine-N-[methoxy(polyethylene glycol)-2000] (ammonium salt) (DOPE-PEG2k, 880130), 1,2-dioleoyl-sn-glycero-3-phosphoethanolamine-N-(lissamine rhodamine B sulfonyl) (ammonium salt) (DOPE-Rh, 810150), and 1,2-dioleoyl-sn-glycero-3-phosphoethanolamine-N-(7-nitro-2-1,3-benzoxadiazol-4-yl) (ammonium salt) (DOPE-NBD, 810145) were purchased from Avanti Polar Lipids, and all these lipids are dissolved in chloroform. Water was purified via ultrafilter (arium® CellPlus, Sartorius Lab Instruments).

Preparation of aqueous two-phase system (ATPS)

16 w% PEG, 10 w% Dextran and 74 w% water were mixed in a 50 mL Falcon centrifuge tube and then vortexed at 2500 rpm (Agitateurs Vortex, 444-2790, VWR) until fully dissolved. The mixture was then centrifuged at 3070x g for 15 mins (EBA 21 centrifuge, Hettich) to accelerate

the phase separation process. Two clear phases should be seen after centrifugation, and the upper phase is PEG-rich phase while the lower is DEX-rich phase.

Preparation of liposomes

97.5 mol% DOPG, 1.5 mol% DOPE-PEG2k and 1.0 mol% DOPE-Rh (or DOPE-NBD) were mixed in a glass vial (50 x 12 mm, 1481-1582, Fisher Scientific) to form a mixture containing 2.5 mg of lipids. For unPEGylated liposomes, 99 mol% DOPG and 1 mol% DOPE-Rh were used. Chloroform in the mixture was evaporated using a nitrogen stream to form a thin lipid film within the vial, then the vial was put in a vacuum desiccator for at least 2 hours to further remove residual chloroform. The anhydrous lipid film was hydrated with 1 mL PEG-rich phase to produce a solution with a lipid concentration of 2.5 mg/mL. This solution was firstly processed with five free-thaw cycles and then extruded with 11 passes through a 0.1 μm filter (Whatman filters, Avanti Mini-Extruder) to produce liposomes. The liposomes were characterized via transmission electron microscopy (JEM-2100F (JEOL, Ltd) fitted with an Orius SC1000 CCD Camera (Gatan, Inc.) and dynamic light scattering (Zetasizer Ultra, Malvern Panalytical) respectively (Supplementary Fig.1).

Emulsion stability

A 242.5 μL liposome solution, 727.5 μL PEG-rich phase, and 30 μL DEX-rich phase were mixed in a cuvette. For control assay with no liposomes, 970 μL PEG-rich phase and 30 μL DEX-rich were used. The above mixture was mixed using a pipette to achieve thorough mixing, and then the absorbance change was monitored using a UV-visible spectrophotometer (Biochrom Libra S32PC UV/Vis Spectrophotometer, Biochrom Libra Instruments) at 650 nm for 8 h.

Droplet imaging and analysis

To create a mixture with various liposome concentrations, a 4-16 μL liposome solution and 178-190 μL PEG-rich phase were added into a 0.5 mL centrifuge tube respectively, while the volume of DEX-rich phase was fixed at 6 μL (total mixture volume was 200 μL). The mixture was vortexed at 2500 rpm for 30 s to produce a uniform emulsion. After that, this emulsion was transferred into a chamber (PMMA, 10mm diameter x 2 mm depth, fabricated via laser cutting platform, ADVL-01039, Universal Laser Systems) for imaging. Images were acquired with an Olympus microscope (IX81, IX2-ILL100, Olympus) or a Nikon microscope (Eclipse TE2000-E, Nikon) in 8-bit type at 1024x1024 resolution and saved as .tiff files. The magnification scales varied from 2x to 20x. Rhodamine and NBD filter sets were used respectively to measure corresponding fluorescence level. The images were then processed using ImageJ and colour was applied to facilitate data analysis. Merged images were generated via merge channel in ImageJ, and the brightness and contrast were subsequently adjusted for clarity. To analyse droplet stability, droplet diameter was measured for at least 50 droplets that were chosen stochastically within each image. All images used were obtained from the fluorescence channel.

Droplet velocity and liposome coating intensity

100 μL of 0.10 mg/mL emulsion was transferred into a chamber and left for 1h to obtain stable emulsion droplets. Then, 50 μL of pure water was added into this chamber to induce droplet motion. Olympus microscope (IX81, IX2-ILL100, Olympus) or Nikon microscope (Eclipse TE2000-E,Nikon) was used to monitor the whole process. For recording, image stacks were acquired in 8-bit type at 1024x1024 resolution and saved as .tiff files. Droplets trajectory and velocity were measured using ImageJ (Fiji ImageJ>Plugins>Tracking>Manual Tracking).

To measure the fluorescence intensity of liposome coatings, a concentric circle equivalent to the droplet diameter was drawn to encircle the droplet, and that circle then was added into ROI

manager for measurement (Fiji ImageJ>Analyze>Tools>ROI manager>Measure). The measurement result includes circle area, mean intensity, minimum intensity, and maximum intensity. For each droplet, the difference between mean intensity and minimum intensity can be seen as the intensity of liposome coating. The height of the dark droplet part (droplet surface without liposome coating) was measured manually by drawing auxiliary lines.

Data availability. All relevant data are available from the corresponding author on reasonable request.

References

1. Li J*, et al.* Micromotors Spontaneously Neutralize Gastric Acid for pH-Responsive Payload Release. *Angew Chem Int Ed Engl* **56**, 2156-2161 (2017).
2. Pouponneau P, Bringout G, Martel S. Therapeutic magnetic microcarriers guided by magnetic resonance navigation for enhanced liver chemoembilization: a design review. *Ann Biomed Eng* **42**, 929-939 (2014).
3. Xiao Y*, et al.* Moving Droplets in 3D Using Light. *Adv Mater* **30**, e1801821 (2018).
4. Li T, Li L, Song W, Wang L, Shao G, Zhang G. Self-Propelled Multilayered Microrockets for Pollutants Purification. *ECS J Solid State Sci Technol* **4**, S3016-S3019 (2015).
5. Tong J*, et al.* Visible-Light-Driven Water-Fueled Ecofriendly Micromotors Based on Iron Phthalocyanine for Highly Efficient Organic Pollutant Degradation. *Langmuir*, (2019).
6. Wang L, Song S, van Hest J, Abdelmohsen L, Huang X, Sanchez S. Biomimicry of Cellular Motility and Communication Based on Synthetic Soft-Architectures. *Small*, e1907680 (2020).
7. Buddingh BC, van Hest JCM. Artificial Cells: Synthetic Compartments with Life-like Functionality and Adaptivity. *Acc Chem Res* **50**, 769-777 (2017).
8. Lu AX*, et al.* Catalytic propulsion and magnetic steering of soft, patchy microcapsules: ability to pick-up and drop-off microscale cargo. *ACS Appl Mater Interfaces* **8**, 15676-15683 (2016).
9. Chen A, Ge XH, Chen J, Zhang L, Xu JH. Multi-functional micromotor: microfluidic fabrication and water treatment application. *Lab Chip* **17**, 4220-4224 (2017).
10. Sun J, Mathesh M, Li W, Wilson DA. Enzyme-Powered Nanomotors with Controlled Size for Biomedical Applications. *ACS Nano* **13**, 10191-10200 (2019).
11. Joseph A*, et al.* Chemotactic synthetic vesicles: Design and applications in blood-brain barrier crossing. *Sci Adv* **3**, e1700362 (2017).
12. Palacci J, Sacanna S, Vatchinsky A, Chaikin PM, Pine DJ. Photoactivated colloidal dockers for cargo transportation. *J Am Chem Soc* **135**, 15978-15981 (2013).
13. Dai B*, et al.* Programmable artificial phototactic microswimmer. *Nat Nanotechnol* **11**, 1087-1092 (2016).
14. Pacheco M, Sanchez BJ, Escarpa A. Visible light driven Janus microvehicles in biological media. *Angew Chem Int Ed Engl* **58**, 18017-18024 (2019).

15. Villa K, Novotny F, Zelenka J, Browne MP, Ruml T, Pumera M. Visible-Light-Driven Single-Component BiVO4 Micromotors with the Autonomous Ability for Capturing Microorganisms. *ACS Nano* **13**, 8135-8145 (2019).
16. Yu S*, et al.* Self-Propelled Janus Microdimer Swimmers under a Rotating Magnetic Field. *Nanomaterials (Basel)* **9**, 1672 (2019).
17. Jurado-Sanchez B, Pacheco M, Rojo J, Escarpa A. Magnetocatalytic Graphene Quantum Dots Janus Micromotors for Bacterial Endotoxin Detection. *Angew Chem Int Ed Engl* **56**, 6957-6961 (2017).
18. Lancia F, Yamamoto T, Ryabchun A, Yamaguchi T, Sano M, Katsonis N. Reorientation behavior in the helical motility of light-responsive spiral droplets. *Nat Commun* **10**, 5238 (2019).
19. Chen YJ, Nagamine Y, Yoshikawa K. Self-propelled motion of a droplet induced by Marangoni-driven spreading. *Phys Rev E* **80**, 016303 (2009).
20. M. HM, T. T, T. I, N. P, T. S. Fatty Acid Chemistry at the Oil-Water Interface Self-Propelled Oil Droplets. *J Am Chem Soc* **129**, 9386-9391 (2007).
21. Suematsu NJ, Saikusa K, Nagata T, Izumi S. Interfacial Dynamics in the Spontaneous Motion of an Aqueous Droplet. *Langmuir* **35**, 11601-11607 (2019).
22. Mukouyama Y*, et al.* Self-Propelled Motion of a Nitrobenzene Droplet on Au Electrode during Sn Electrodeposition: Factors Creating Imbalance of Interfacial Tension and Marangoni Effect. *J Electrochem Soc* **165**, H473-H480 (2018).
23. Li M, Brinkmann M, Pagonabarraga I, Seemann R, Fleury J-B. Spatiotemporal control of cargo delivery performed by programmable self-propelled Janus droplets. *Commun Phys* **1**, 1-8 (2018).
24. Ban T, Yamada T, Aoyama A, Takagi Y, Okano Y. Composition-dependent shape changes of self-propelled droplets in a phase-separating system. *Soft Matter* **8**, 3908-3916 (2012).
25. Ban T, Aoyama A, Matsumoto T. Self-generated Motion of Droplets Induced by Korteweg Force. *Chem Lett* **39**, 1294-1296 (2010).
26. Crowe CD, Keating CD. Liquid-liquid phase separation in artificial cells. *Interface Focus* **8**, 20180032 (2018).
27. Iqbal M*, et al.* Aqueous two-phase system (ATPS): an overview and advances in its applications. *Biol Proced Online* **18**, 18 (2016).
28. Zafarani-Moattar MT, Hamzehzadeh S, Nasiri S. A new aqueous biphasic system containing polypropylene glycol and a water-miscible ionic liquid. *Biotechnol Prog* **28**, 146-156 (2012).
29. Mazzola PG*, et al.* Liquid–liquid extraction of biomolecules: an overview and update of the main techniques. *J Chem Technol Biotechnol* **83**, 143-157 (2008).
30. Hatti-Kaul R. *Aqueous two-phase systems: methods and protocols*. Springer Science & Business Media (2000).
31. Mitrea DM, Kriwacki RW. Phase separation in biology; functional organization of a higher order. *Cell Commun Signal* **14**, 1 (2016).
32. Cacace DN, Rowland AT, Stapleton JJ, Dewey DC, Keating CDJL. Aqueous emulsion droplets stabilized by lipid vesicles as microcompartments for biomimetic mineralization. *Langmuir* **31**, 11329-11338 (2015).
33. Dominak LM, Gundermann EL, Keating CD. Microcompartmentation in artificial cells: pH-induced conformational changes alter protein localization. *Langmuir* **26**, 5697-5705 (2010).
34. Dewey DC, Strulson CA, Cacace DN, Bevilacqua PC, Keating CD. Bioreactor droplets from liposome-stabilized all-aqueous emulsions. *Nat Commun* **5**, 4670 (2014).

35. Asenjo JA, Andrews BA. Aqueous two-phase systems for protein separation: a perspective. *J Chromatogr A* **1218**, 8826-8835 (2011).
36. M. Scott Long CDJ, Marcus R. Helfrich, Lauren K. Mangeney-Slavin, and Christine D. Keating. Dynamic microcompartmentation in synthetic cells. *Proc Natl Acad Sci U S A* **102**, 5920-5925 (2004).
37. Strulson CA, Molden RC, Keating CD, Bevilacqua PC. RNA catalysis through compartmentalization. *Nat Chem* **4**, 941-946 (2012).
38. Long MS, Keating CD. Nanoparticle conjugation increases protein partitioning in aqueous two-phase systems. *Anal Chem* **78**, 379-386 (2006).
39. Marcus R. Helfrich LKM-S, M. Scott Long, Karrera Y. Djoko, and Christine D. Keating. Aqueous Phase Separation in Giant Vesicles. *J Am Chem Soc* **124**, 13374-13375 (2002).
40. Hindley JW*, et al.* Building a synthetic mechanosensitive signaling pathway in compartmentalized artificial cells. *Proc Natl Acad Sci U S A* **116**, 16711-16716 (2019).
41. Hindley JW*, et al.* Light-triggered enzymatic reactions in nested vesicle reactors. *Nat Commun* **9**, 1-6 (2018).
42. Bolognesi G*, et al.* Sculpting and fusing biomimetic vesicle networks using optical tweezers. *Nat commun* **9**, 1-11 (2018).
43. Papahadjopoulos D, Portis A, Pangborn W. Calcium-induced lipid phase transitions and membrane fusion. *Ann N Y Acad Sci* **308**, 50-66 (1978).
44. Liu Y, Lipowsky R, Dimova R. Concentration dependence of the interfacial tension for aqueous two-phase polymer solutions of dextran and polyethylene glycol. *Langmuir* **28**, 3831-3839 (2012).
45. Davis RE, Acrivos A. The influence of surfactants on the creeping motion of bubbles. *Chem Eng Sci* **21**, 681-685 (1966).
46. Levich VG. (1962). Physicochemical Hydrodynamics. New Jersey: Prentice-Hall, Englewood Cliffs.
47. Savic P. Report MT22. Division of Mechanical Engineering, National Research Council of Canada, (1953).
48. Levich VG. Diffusion kinetics theory of heterogeneous chemical processes. *Z Fiz Khim* **22**, 721-729 (1948).

Acknowledgements

This work was supported by Department of Chemistry at Imperial College London. SZ would like to thank the China Scholarship Council (CSC) for the financial support. CC would like to thank the Wellcome Trust Institutional Strategic Supporting Fund for their financial support through an ISSF Springboard Fellowship. This work was supported by an Engineering and Physical Sciences Research Council (EPSRC) Doctoral Prize Fellowship awarded to JWH, and a UKRI Future Leaders Fellowship grant reference MR/S031537/1 awarded to YE.

Author contributions

CC performed the TEM and DLS experiments. SZ performed other experiments and the data analysis. GB performed the theoretical analysis of droplet motion. SZ, CC, JWH, GB, YE and OC contributed to designing the experiments, discussion and writing the manuscript.

Additional information

Supplementary Information is available for this paper.

Competing interest: The authors declare no competing interests.

Figures

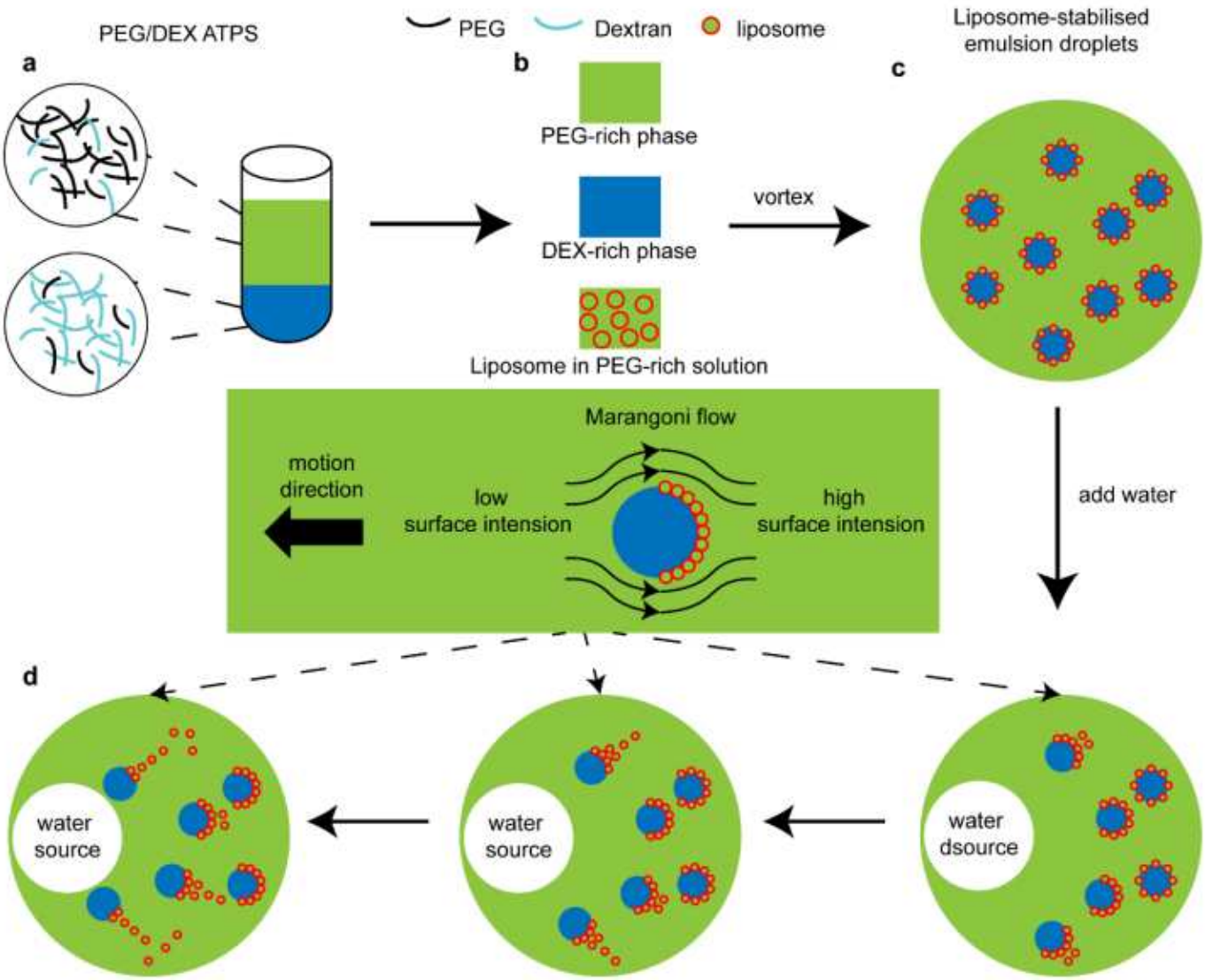

Figure 1

Illustration for the main content. (a) PEG/DEX solution separates into PEG-rich and DEX-rich phase. (b) Preparation of liposome in PEG-rich solution. (c) Preparation of emulsion droplets by mixing PEG-rich phase, DEX-rich phase, and liposomes via vortex. (d) Droplets achieve directional motion towards the water source in respond to a polymer gradient caused by the addition of water.

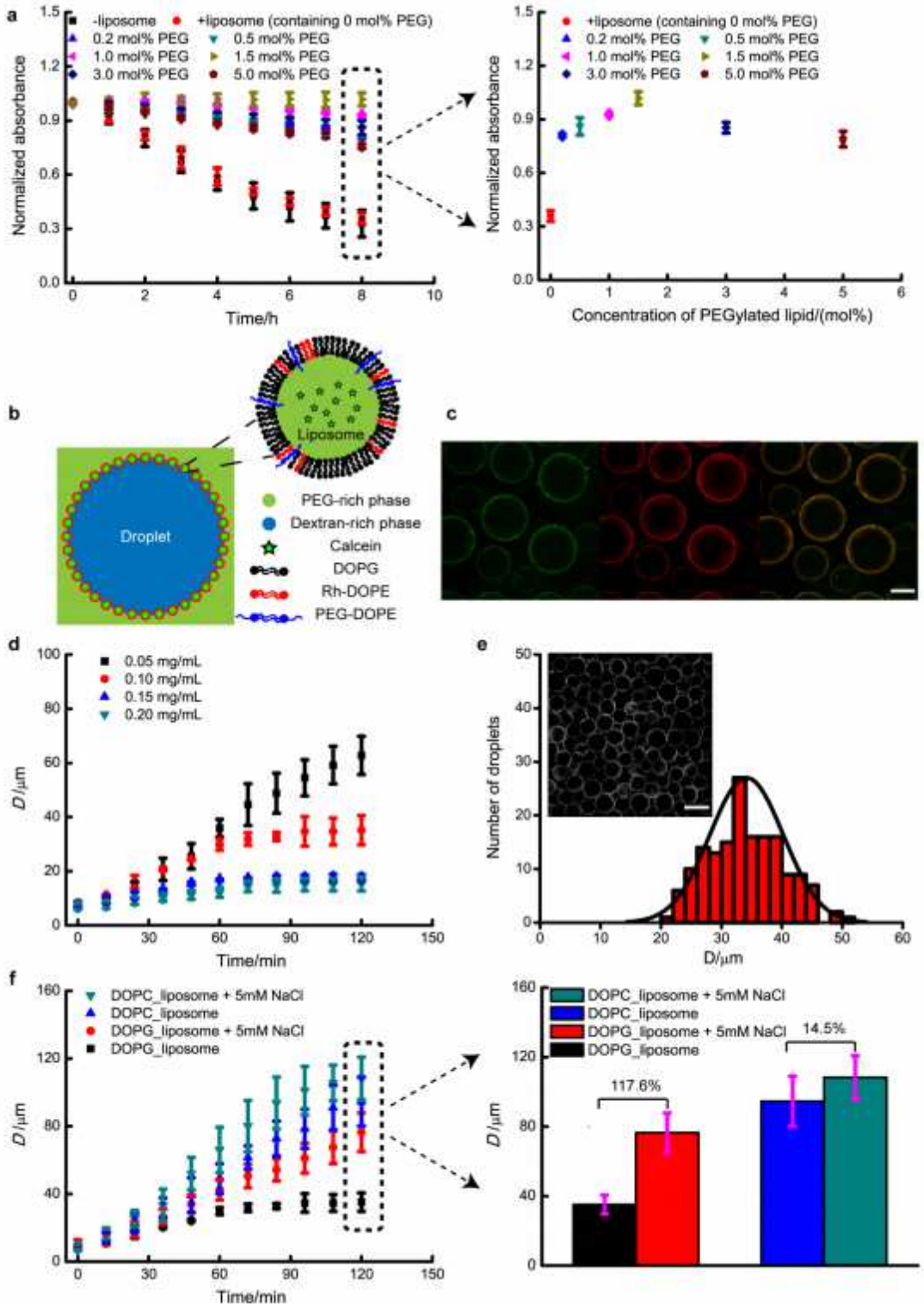

Figure 2

Characterisation of droplet morphology and stability. (a) Emulsion absorbance change during 8 h. If emulsions stay stable, it should remain turbid during observation, i.e. the absorbance remain unchanged. Or a decrease in absorbance can be observed for unstable emulsions. Final absorbance at 8 h was extracted for quantitative analysis. (b) Illustration for liposome-stabilise droplet. (c) Droplets stabilized by Calcein-containing (5mM) liposomes. From left to right, Calcein channel, Rhodamine channel, and merger

channel. Colours were added via Image J. Liposome solution is diluted after size exclusion, which leads to the large droplet size. Scale bar is 50 ⍰⍰m. (d) Effect of liposome concentration on droplet stability. (e) Droplet size distribution for stable droplets (stabilised with DOPG-liposomes). The inset picture corresponds to droplets at 120 min for 0.10 mg/mL in (d). Scale bar is 50 ⍰⍰m. (f) Effect of liposome type and salt addition on droplet stability. Droplet diameter at 120 min was extracted to draw a histogram in order to show the difference of salt addition on different liposome-stabilised droplets. Error bars represent 1 s.d. (n = 3) for each data set.

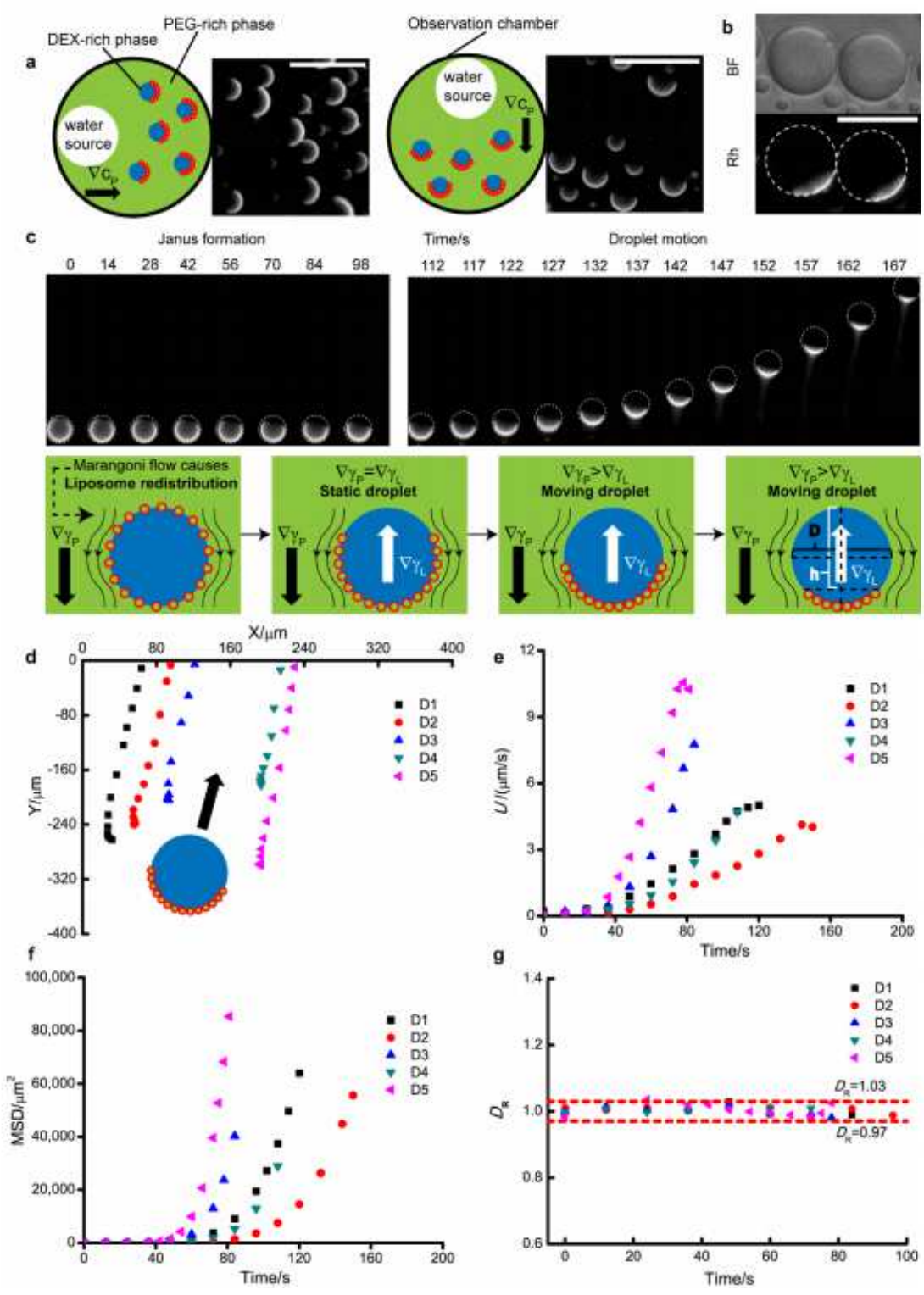

Figure 3

Formation of Janus droplets and subsequent droplet motion. (a) Janus conformation is relevant with the position of water addition. Pictures were extracted from video 1 and 2 and cropped for better presentation. □□□□□□ is the polymer gradient. (b) Droplet structure under bright field (BF) or Rhodamine fluorescence channel (Rh). (c) Janus formation and droplet motion. In respond to water gradient, the droplet gradually transformed into Janus droplet. When the ratio of h to D reached approximate 0.3, the droplet starts a directional motion towards the water source, with a characteristic tail of liposomes due to liposome desorption from the droplet surface during the motion. □□□□□□ and □□□□□□ are the IFT gradients caused by polymer gradient and liposomes respectively. Frames were extracted from video 1 and cropped for better presentation. (d) Trajectories of moving droplets. D1-D5 are representative droplets stochastically chosen from video 1. Arrow corresponds to the direction of movement. (e) Corresponding velocity , (f) MSD and (g) diameter change (the ratio of droplet diameter at different time points to its average diameter during motion was taken as normalized diameter, i.e. DR) for droplets in (d). The time points when droplets start moving were chosen as time zero. Scale bar is 50 □□m for (a)-(c).

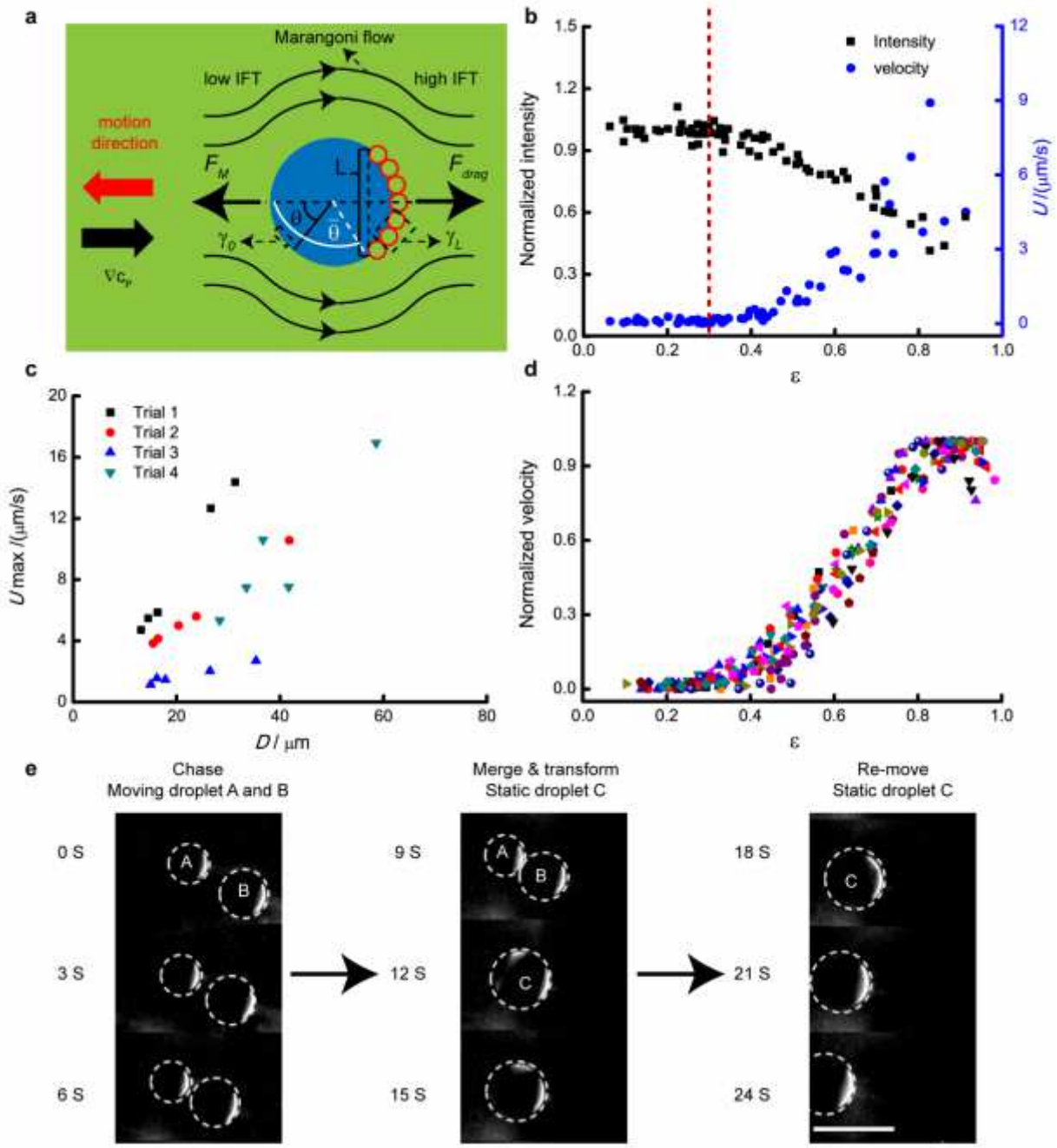

Figure 4

Mechanism behind motion. (a) Illustration for the Marangoni effect. (b) The total intensity of liposome coating and corresponding droplet velocity for different droplets. (c) The relationship between maximum velocity and droplet diameter. The correlation coefficient for trail 1-4 is 0.99, 0.99,0.96, 0.85. (d) The relationship between normalized velocity and the value of □□ (h/D). 20 droplets from 4 trials were chosen for analysis. (e) Chasing and merge process for two droplets with different diameter. Pictures were extracted from video 6 and cropped for better presentation. Scale bar is 50 □□m.

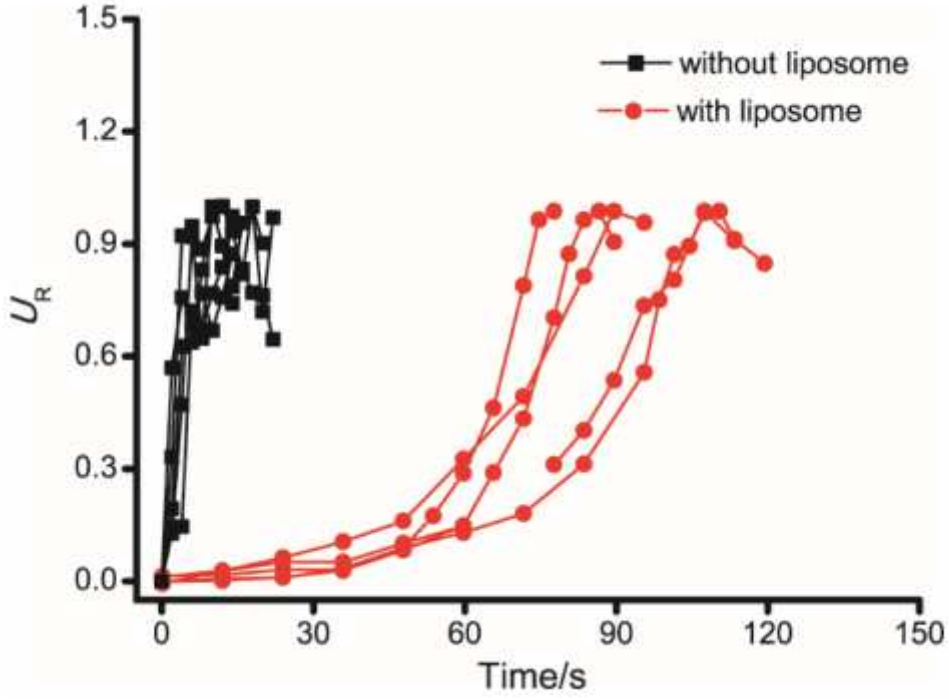

Figure 5

Effect of liposome coating on droplet motion. Emulsion droplets were prepared with/without liposomes, and water was added to induce droplet motion. 5 droplets with or without liposome were chosen from different trials for analysis. The ratio of droplet velocity at different time points to its maximum velocity was taken as relative velocity (□□□□).

Supplementary Files

This is a list of supplementary files associated with this preprint. Click to download.

- SupplementaryInformation.docx